AVO-sensitive semblance analysis for wide-azimuth data

Jia Yan & Ilya Tsvankin
Center for Wave Phenomena, Department of Geophysics, Colorado School of Mines

ABSTRACT

Conventional semblance-based moveout analysis models prestack reflection data with events that have hyperbolic moveout and no amplitude variation with offset (AVO). It has been shown that substantial amplitude variation and even phase change with offset do not significantly compromise the semblance operator. However, polarity reversal associated with a change in the sign of the reflection coefficient may cause conventional semblance to fail. An existing modification of the semblance operator that takes amplitude variations into account (so-called "AK semblance") is limited to narrow-azimuth data and cannot handle nonhyperbolic moveout.

Here, we extend the AK semblance algorithm to long-spread (nonhyperbolic) moveout and 3D multiazimuth data. To preserve velocity resolution in the presence of substantial AVO signature, we keep the ratio K of the AVO gradient and intercept constant within each semblance window. In the presence of azimuthal anisotropy, however, the parameter K has to be azimuthally dependent. In our implementation, the modified semblance operator is combined with a nonhyperbolic moveout inversion algorithm devised for wide-azimuth data.

Synthetic tests confirm that the distortions in moveout analysis caused by polarity reversals are more common for long-spread data. Conventional semblance produces substantial errors in both the NMO ellipse and azimuthally varying parameter η not just for type 2 AVO response, but also for some models with type 1 AVO. In contrast, the AK semblance algorithm gives accurate estimates of the moveout parameters even when the position of the polarity reversal varies with azimuth. The AK method not only helps to flatten wide-azimuth reflection events prior to stacking and azimuthal AVO analysis, but also provides input parameters for the anisotropic geometrical-spreading correction.

Key words: AVO, polarity reversal, semblance, wide-azimuth, anisotropy

1 INTRODUCTION

Semblance-based moveout analysis is routinely employed in seismic data processing to estimate stacking (moveout) velocity $V_{\rm nmo}$ as a function of the zero-offset time t_0 (e.g., Taner and Koehler, 1969). NMO velocity, which typically represents the most stable parameter constrained by surface seismic data, is then used to build the initial velocity model and flatten reflection events for subsequent processing.

The conventional semblance operator can be written as

$$S(V,\ t_0) = \frac{\displaystyle\sum_{t_1}\left[\sum_{x} D_V\,(t_1,x)\right]^2}{N\displaystyle\sum_{t_1}\sum_{x} D_V^2\,(t_1,x)}\,, \qquad (1)$$

where t_1 are the zero-offset times within a time window centered at t_0, x is the source-to-receiver offset, N is the number of traces in a CMP (common mid-

point) gather, and D_V represents the data picked along hyperbolic moveout curves computed with the velocity $V = V_{\rm nmo}$.

Despite its general robustness, the operator in equation 1 has two serious limitations. First, it does not not account for deviations from hyperbolic moveout, which become significant for offset-to-depth ratios greater than unity. To make equation 1 suitable for long-spread reflection events, the conventional hyperbolic moveout equation is replaced by more complicated nonhyperbolic functions, such as those developed by Tsvankin and Thomsen (1994) and Alkhalifah and Tsvankin (1995).

Second, the semblance operator 1 is devised under the assumption that reflection amplitudes are constant and, therefore, includes no allowance for amplitude variation with offset (AVO). Still, conventional semblance usually estimates moveout velocity with sufficient accuracy even for events with relatively strong AVO, as long as there is no polarity reversal within the recorded offset range. In the presence of polarity reversals, however, the conventional operator often fails and gives a strongly distorted NMO-velocity value (Sarkar et al., 2001). Then the reflection event cannot be properly flattened, which leads to a poor-quality, low-frequency stack.

Figure 1 displays three common types of P-wave AVO behavior for gas sands described in Rutherford and Williams (1989). Classes 1 and 2 correspond to highly or moderately compressed sands beneath shales, while class 3 sands are overlaid by a more compressed overburden. Evidently, for class 1 and class 2 responses a polarity reversal occurs at incidence angles less than 30°. Furthermore, the influence of anisotropy increases the chance of observing polarity reversals on conventional-spread reflection data. Indeed, most shale formations are transversely isotropic (TI), and for typical positive values of the Thomsen (1986) parameter δ in shales the AVO gradient increases by absolute value (Kim et al., 1993; Tsvankin, 2005). As a result, the polarity reversal for the interface between gas sands and VTI (TI with a vertical symmetry axis) shales moves towards lower angles from its "isotropic" position (Figure 1).

Sarkar et al. (2002) developed the so-called "AK semblance" method to make velocity analysis suitable for data with polarity reversals. Their approach is based on introducing into the semblance operator a smooth amplitude variation with offset governed by two parameters (A and K). The existing AK algorithm, however, is designed for 2D data and is restricted to the hyperbolic portion of the moveout curve (i.e., to conventional-length spreads).

Here, we present an extension of the AK semblance method to nonhyperbolic (long-spread) moveout and wide-azimuth data. Our generalized AK algorithm is particularly important for processing of reflection data from anisotropic media because anisotropy usually enhances nonhyperbolic moveout of P-waves (Tsvankin, 2005) and moves the polarity reversal toward smaller offsets (see above). Also, amplitude variations with offset and azimuth may substantially distort the results of moveout analysis for wide-azimuth surveys acquired above fractured formations. Vasconcelos and Tsvankin (2006) presented an efficient technique for nonhyperbolic moveout inversion of wide-azimuth data from layered azimuthally anisotropic media, but their semblance operator does not take amplitude variations into account.

Table 1. Model parameters for the three types of AVO responses in Figure 1.

		V_P(km/s)	V_S(km/s)	ρ (g/cm^3)
Layer 1		3.00	1.32	2.4
Layer 2	type 1	4.40	2.80	2.0
	type 2	3.75	2.40	2.0
	type 3	2.95	1.89	2.0

We begin by reviewing the AK semblance algorithm of Sarkar et al. (2002) and its implementation in moveout analysis. Then we extend the AK semblance operator to long-offset data using the nonhyperbolic moveout equation of Alkhalifah and Tsvankin (1995). To apply the method to wide-azimuth data, we make the AVO gradient azimuthally dependent and incorporate it into the moveout-inversion algorithm of Vasconcelos and Tsvankin (2006). Synthetic tests for VTI and azimuthally anisotropic (orthorhombic) models demonstrate the superior performance of the generalized AK semblance for both class 1 and 2 AVO responses.

2 METHODOLOGY

As discussed above, the conventional semblance operator in equation 1 does not account for amplitude variations within the CMP gather. A more general semblance formulation for 2D data was introduced by Sarkar et al. (2002):

$$S_G(V,\ t_0) = 1 - \frac{\parallel M - D_V \parallel^2}{\parallel D_V \parallel^2}\,, \qquad (2)$$

where t_0, as before, is the zero-offset time at the center of the semblance window, $D_V = D_V(t_1, x)$ is the data with the zero-offset time t_1 after a hyperbolic moveout correction with the velocity $V = V_{\rm nmo}$, and $M = M(t_1, x)$ is the modeled variation of the trace amplitudes. The amplitude parameters that govern $M(t_1, x)$ and the velocity $V_{\rm nmo}$ are estimated by matching the model M and data D, which can be achieved by maximizing the semblance (i.e., by minimizing $\parallel M - D_V \parallel^2$). The generalized semblance from equation 2 reduces to the conventional semblance operator (equation 1) when the am-

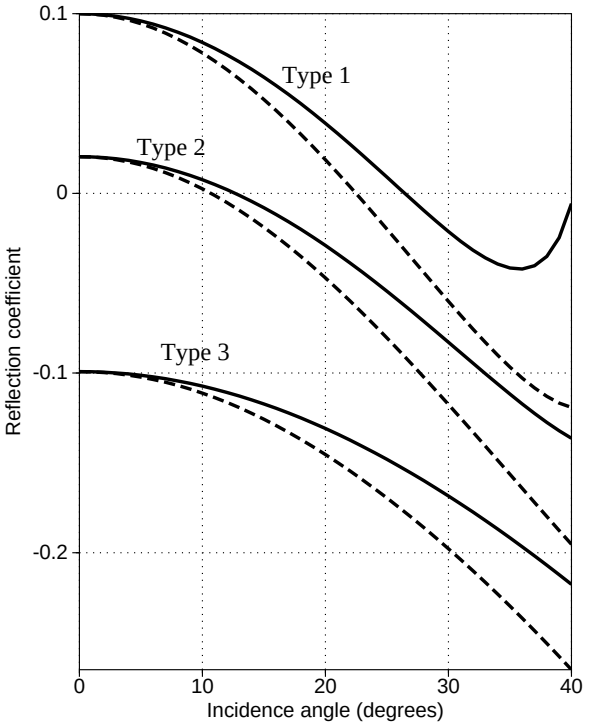

Figure 1. Three types of P-wave AVO responses (reflection coefficients) computed from exact equations (Rüger, 2001) for gas sands overlaid by shale. The solid lines correspond to the three isotropic models from Table 1 (Rutherford and Williams, 1989). The dashed lines are computed for models with the same vertical velocities and densities, but the shale layer is VTI with the Thomsen parameters $\epsilon = \delta = 0.2$. All three models have negative AVO gradients, which become larger by absolute value when the shale is anisotropic.

plitudes associated with model M are independent of offset (Sarkar et al., 2002).

The offset-dependent function M in the AVO-sensitive semblance algorithm can be approximately described by Shuey's (1985) linearized equation for the reflection coefficient:

$$\begin{aligned} M(t_1, x) &= A(t_1) + B(t_1) \sin^2 \theta_x \\ &\approx A(t_1) + B(t_1) \, \frac{x^2}{x^2 + V_{\rm nmo}^2 \, t_0^2} \, , \end{aligned} \tag{3}$$

where $A(t_1)$ and $B(t_1)$ are the AVO intercept and gradient (respectively) for the reflection event with the zero-offset time t_1, and θ_x is the phase angle of incidence at the reflector, which is expressed through offset x under the assumption that the medium is homogeneous and isotropic.

The exact incidence angle θ_x cannot be computed without knowledge of the velocity model. It should be emphasized, however, that there is no need for an accurate estimate θ_x, because the only role of equation 3 is to introduce a smooth amplitude variation with offset into the semblance operator. Note that Shuey's (1985) equation cannot represent measured reflection amplitudes anyway because it does not include the source directivity and such propagation factors as the geometrical spreading and transmission coefficients along the raypath.

As pointed out by Sarkar et al. (2002), equation 3 (called "AB semblance") allows too much freedom to fit events with various combinations of incorrect parameters A, B, and $V_{\rm nmo}$, which results in poor velocity resolution. To reduce this interplay, Sarkar et al. (2002) suggested to keep the ratio $A/B = K$ constant inside the semblance window, which implies that the wavelet shape does not change with offset:

$$M(t_1, x) = A(t_1) \left(1 + K \, \frac{x^2}{x^2 + V_{\rm nmo}^2 \, t_0^2} \right) . \tag{4}$$

Modeling data using equation 4 with $K = const$ is referred to by Sarkar et al. (2002) as "AK semblance."

The semblance window follows the traveltime trajectory computed from an analytic (hyperbolic in the work by Sarkar et al., 2002) moveout equation and has the width close to the length of the wavelet. For a window with N_t sampling points, the AK semblance operator has only $N_t + 1$ parameters (as compared to $2N_t$ for AB semblance), which mitigates the tradeoffs and increases velocity resolution.

For a given zero-offset time t_0 and a trial velocity $V_{\rm nmo}$, the parameters A and K can be found analytically by setting the derivatives of S_G with respect to A and K to zero (see Appendix A). The obtained expressions are then substituted back into equation 2 to compute the generalized semblance. As in conventional semblance algorithms, scanning over $V_{\rm nmo}$ is used to maximize the semblance and estimate the best-fit moveout (stacking) velocity.

A key issue in the implementation of the generalized semblance algorithm is the choice of the moveout equation $t(x)$. Reflection moveout on conventional-length spreads (i.e., for offset-to-depth ratios not much larger than unity) typically is close to hyperbolic:

$$t^2(x) = t_0^2 + \frac{x^2}{V_{\rm nmo}^2} \, . \tag{5}$$

Although equation 3 is widely used in seismic processing, it breaks down at longer offsets, especially if the medium is anisotropic. A more accurate, nonhyperbolic moveout equation for P-wave data in VTI media was suggested by Alkhalifah and Tsvankin (1995):

$$t^2(x) = t_0^2 + \frac{x^2}{V_{\rm nmo}^2} - \frac{2\eta \, x^4}{V_{\rm nmo}^2 \left[t_0^2 \, V_{\rm nmo}^2 + (1 + 2\eta) \, x^2 \right]} \, , \tag{6}$$

where $\eta \equiv (\epsilon - \delta)/(1 + 2\delta)$ is the "anellipticity" parameter, which controls P-wave time processing for vertical transverse isotropy. The x^4-term in equation 6 is

proportional to η and describes nonhyperbolic moveout for large offsets. Below we employ the Alkhalifah-Tsvankin equation in the AK semblance operator to perform moveout analysis of long-spread 2D P-wave data.

The main goal of the paper, however, is to extend the principle of AK semblance to wide-azimuth surveys, which are often acquired for purposes of fracture detection. Reservoirs with vertical fracture sets are commonly described by an effective anisotropic model with orthorhombic symmetry (Schoenberg and Helbig, 1997; Bakulin et al., 2000; Grechka and Kachanov, 2006). Azimuthally dependent P-wave reflection traveltimes in a horizontal orthorhombic layer can be well-approximated by a generalized version of equation 6, in which both the NMO velocity and parameter η vary with the azimuth α (Xu et al., 2005; Vasconcelos and Tsvankin, 2006):

$$\begin{aligned} t^2(x,\alpha) &= t_0^2 + \frac{x^2}{V_{\rm nmo}^2(\alpha)} \\ &- \frac{2\eta(\alpha)\, x^4}{V_{\rm nmo}^2(\alpha)\,[t_0^2\, V_{\rm nmo}^2(\alpha) + (1+2\eta(\alpha))\, x^2]}\,, \end{aligned} \tag{7}$$

where $V_{\rm nmo}$ is obtained from the equation of the NMO ellipse:

$$V_{\rm nmo}^{-2}(\alpha) = \frac{\cos^2(\alpha-\varphi)}{\left[V_{\rm nmo}^{(2)}\right]^2} + \frac{\sin^2(\alpha-\varphi)}{\left[V_{\rm nmo}^{(1)}\right]^2}\,. \tag{8}$$

Here, φ is the azimuth of the $[x_1, x_3]$ symmetry plane, and $V_{\rm nmo}^{(1)}$ and $V_{\rm nmo}^{(2)}$ are the NMO velocities in the symmetry planes $[x_2, x_3]$ and $[x_1, x_3]$, respectively. [The superscript in $V_{\rm nmo}^{(1)}$ and $V_{\rm nmo}^{(2)}$ refers to the axis orthogonal to the corresponding plane; for a detailed discussion of notation, see Tsvankin (1997, 2005).]

The azimuthal variation of the parameter η is approximately given by (Pech and Tsvankin, 2004)

$$\begin{aligned} \eta(\alpha) &= \eta^{(2)}\cos^2(\alpha-\varphi) + \eta^{(1)}\sin^2(\alpha-\varphi) \\ &- \eta^{(3)}\cos^2(\alpha-\varphi)\sin^2(\alpha-\varphi)\,, \end{aligned} \tag{9}$$

where $\eta^{(1)}$, $\eta^{(2)}$, and $\eta^{(3)}$ are the anellipticity parameters defined (respectively) in the $[x_2, x_3]$, $[x_1, x_3]$, and $[x_1, x_2]$ symmetry planes.

The accuracy of equation 7 in both vertical symmetry planes is the same as that in the corresponding equivalent VTI medium. Xu et al. (2005) and Vasconcelos and Tsvankin (2006) show that equations 7–9 provide a close approximation for long-spread P-wave traveltimes recorded in all azimuthal directions, even for strongly anisotropic orthorhombic models. Furthermore, if $V_{\rm nmo}^{(1,2)}$ and $\eta^{(1,2,3)}$ are treated as effective parameters, the same formalism can be applied to P-wave moveout from layered orthorhombic media with uniform orientation of the symmetry planes.

Vasconcelos and Tsvankin (2006) used equations 7–9 to develop an efficient semblance-based moveout-inversion algorithm designed to estimate the parameters φ, $V_{\rm nmo}^{(1,2)}$ and $\eta^{(1,2,3)}$ from wide-azimuth P-wave data. Their method, however, does not account for amplitude variation with offset and azimuth and, similar to conventional 2D semblance techniques, can break down in the presence of polarity reversals. Below, we devise a more stable, 3D AK semblance operator by incorporating an azimuthally dependent amplitude function into the semblance computation.

When the medium above or below the reflector is azimuthally anisotropic, the AVO gradient and reflection amplitude as a whole vary with azimuth. For a boundary between two orthorhombic halfspaces with the same orientation of the vertical symmetry planes, the AVO gradient $B(\alpha)$ can be approximated by (Rüger, 2001)

$$B(\alpha) = B^{(2)}\cos^2(\alpha-\varphi) + B^{(1)}\sin^2(\alpha-\varphi)\,, \tag{10}$$

where $B^{(1)}$ and $B^{(2)}$ are the AVO gradients in the $[x_2, x_3]$ and $[x_1, x_3]$ planes, respectively. Then the ratio $K(\alpha)$ of the AVO gradient and intercept also becomes azimuthally dependent and can be written as

$$K(\alpha) = K^{(2)}\cos^2(\alpha-\varphi) + K^{(1)}\sin^2(\alpha-\varphi)\,. \tag{11}$$

Substitution of $K(\alpha)$ from equation 11 into equation 4 yields an azimuthally dependent amplitude function that can be used in the AK semblance computation. In our method, we combine this amplitude function with the moveout equations 7–9 discussed above to devise an AK semblance operator that can handle polarity reversals in wide-azimuth data collected into CMP gathers (see Appendix A). Although equation 11 does not describe geometrical spreading and some other factors that influence recorded amplitudes, it allows us to account for amplitude variation with azimuth $K^{(1)}$, $K^{(2)}$. In particular, it helps to mitigate distortions in the semblance computation related to the azimuthal dependence of the offset that corresponds to the polarity reversal.

Similar to the algorithm of Vasconcelos and Tsvankin (2006), we carry out estimation of $K^{(1)}$, $K^{(2)}$, and the moveout parameters φ, $V_{\rm nmo}^{(1,2)}$ and $\eta^{(1,2,3)}$ in three steps. First, we invert for the NMO ellipse described by φ, $V_{\rm nmo}^{(1)}$, and $V_{\rm nmo}^{(2)}$ using conventional-spread, wide-azimuth data with offsets limited by the reflector depth. If there is an indication of a polarity reversal at the near offsets, we also estimate an azimuthally-invariant value of K along with the NMO ellipse. This step gives initial values of the symmetry-plane azimuths, NMO velocities, and the parameter K. Second, nonhyperbolic AK semblance analysis is carried out in narrow sectors around the identified symmetry planes to find approximate values of $\eta^{(1)}$, $\eta^{(2)}$, $K^{(1)}$, $K^{(2)}$, as well as updated estimates of $V_{\rm nmo}^{(1)}$ and $V_{\rm nmo}^{(2)}$. Third, we carry out 3D nonhyperbolic moveout inversion using the 3D AK semblance operator for all offsets and azimuths in the gather. The search starts with the initial model obtained during the previous steps and scans over φ,

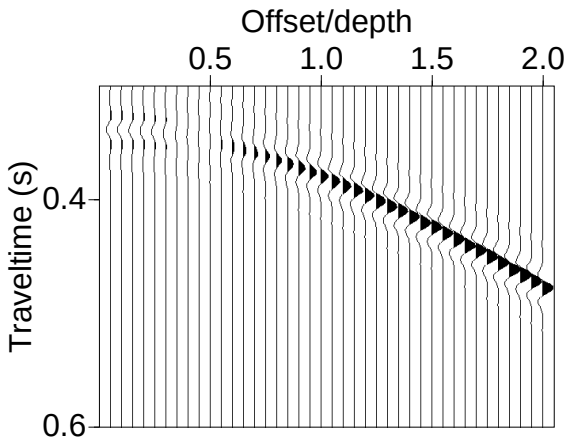

Figure 2. Shot record of a P-wave reflection from an interface between VTI (top) and isotropic (bottom) media. The model parameters are listed in Table 2. The event has a type 2 AVO response with the polarity reversal at an offset-to-depth ratio close to 0.5.

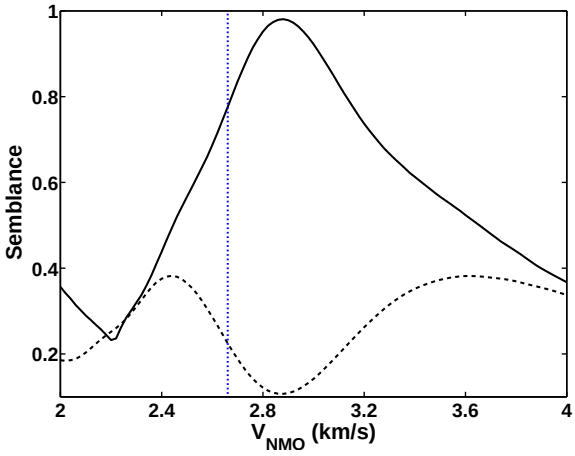

Figure 3. Semblance for the reflection event from Figure 2 computed using the hyperbolic moveout equation 5; the model parameters are listed in Table 2. The dashed curve is produced by the conventional semblance algorithm, and the solid curve is AK semblance. The vertical dotted line marks the actual NMO velocity.

$V_{\rm nmo}^{(1,2)}$, $\eta^{(1,2,3)}$, and $K^{(1,2)}$ to find the best-fit parameters via Powell minimization (Press et al., 1992).

3 TESTS ON SYNTHETIC DATA

Here, the AK semblance algorithm is applied to 2D and 3D long-offset P-wave data from VTI and orthorhombic media. In addition to type 2 AVO responses, for which the polarity reversal is observed at relatively small offsets, we compare the performance of conventional and AK semblance for type 1 AVO. All synthetic data used below are generated by anisotropic ray tracing code ANRAY developed by Gajewski and Pšenčík (1987).

3.1 2D semblance for VTI media

For layer-cake VTI media, each vertical plane is a plane of symmetry, and the semblance analysis can be performed in 2D, for an arbitrary azimuthal direction. We consider a model that includes an isotropic halfspace beneath a VTI layer with relatively small absolute values of the Thomsen parameters ϵ and δ. The anellipticity parameter η, however, is substantial (0.2), which leads to pronounced nonhyperbolic moveout at offsets approaching two reflector depths (Figure 2). The event has a type 2 AVO response (see the discussion above), with relatively low amplitudes at near offsets and the polarity reversal at an offset close to half the reflector depth.

The first test was carried out using the hyperbolic moveout equation in both the conventional and AK semblance operators (Figure 3). Because of the combined influence of the polarity reversal and nonhyperbolic moveout, the conventional operator produces low semblance values for all trial velocities, with the correct velocity close to the semblance *minimum*. Although our algorithm performs much better and yields higher semblance, the best-fit NMO velocity deviates from the actual value. This error, which is caused by the inaccuracy of the hyperbolic moveout equation, can be reduced by muting out long offsets.

In many applications, such as nonhyperbolic moveout inversion and wide-angle AVO analysis, it is necessary to preserve and flatten the far-offset portion of the gather. To improve the traveltime fit at long offsets, next we employ the nonhyperbolic moveout equation 6 in the semblance computation (Figure 4). Although equation 6 provides a close approximation to the exact traveltimes (Alkhalifah and Tsvankin, 1995; Tsvankin, 2005), the best-fit parameters $V_{\rm nmo}$ and η estimated by the conventional semblance algorithm are severely distorted (e.g., the inverted $\eta = 0.72$, while the actual value is 0.2). Clearly, this error is caused by the polarity reversal because the semblance that corresponds to the correct moveout parameters is relatively low. In contrast, AK semblance gives accurate estimates of both $V_{\rm nmo}$ and η, as well as a high semblance value (0.94).

3.2 3D semblance for type 2 AVO

Here, we apply the 3D AK semblance operator to wide-azimuth P-wave reflections from an interface between

Table 2. Parameters of a model that includes VTI (top) and isotropic (bottom) media. The P-wave reflection for this model has a type 2 AVO response. V_{P0} and V_{S0} are the vertical P- and S-wave velocities, respectively.

	V_{P0}(km/s)	V_{S0}(km/s)	ρ (g/cm^3)	ϵ	δ	$V_{\rm nmo}$(km/s)	η
VTI	2.96	1.38	2.43	0.065	-0.096	2.66	0.2
ISO	3.49	2.29	2.14	0	0	3.49	0

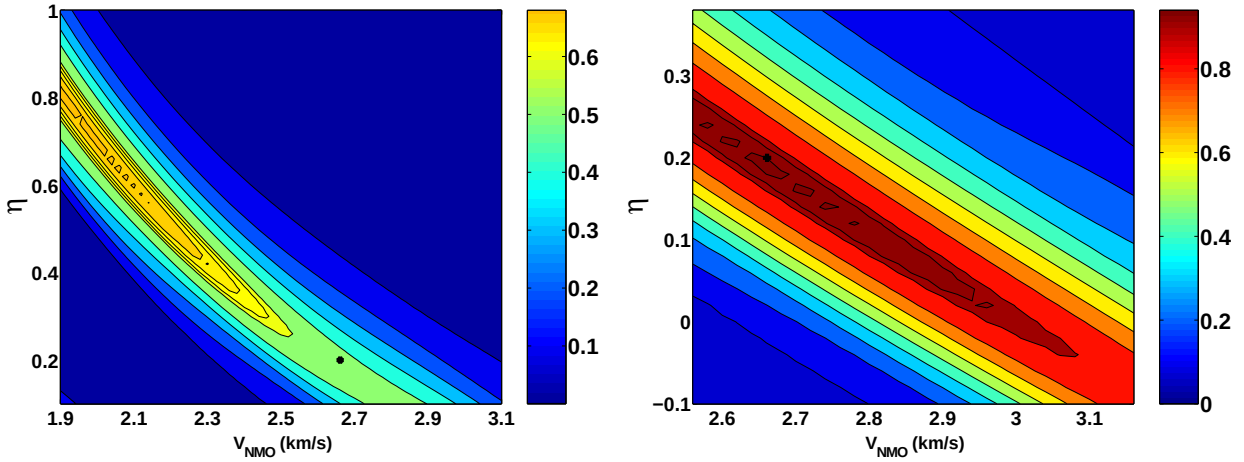

Figure 4. Semblance scans over $V_{\rm nmo}$ and η computed for the event from Figure 2 using the nonhyperbolic moveout equation 6. The scans are generated by the (a) conventional and (b) AK semblance operators. The black dots mark the true model parameters. The best-fit values are $V_{\rm nmo}$ = 1.98 km/s and η = 0.72 for conventional semblance (the maximum semblance is 0.72) and $V_{\rm nmo}$=2.68 km/s, η=0.18 for AK semblance (the maximum semblance is 0.94).

orthorhombic (incidence) and isotropic or orthorhombic (reflecting) media. Since the AVO gradient for this model is azimuthally dependent, the offset of the polarity reversal becomes a function of azimuth as well. If the polarity reversal occurs at relatively small offsets, the corresponding phase incidence angle $\theta_{\rm pr}$ can be estimated by setting $1 + K(\alpha)\sin^2\theta_{\rm pr} = 0$. Using equation 11 with $\varphi = 0$ (i.e., $\alpha = 0$ in the $[x_1, x_3]$-plane), we find

$$\sin^2\theta_{\rm pr} = \frac{-1}{K^{(1)}\,\sin^2\alpha \,+\, K^{(2)}\,\cos^2\alpha}\,. \qquad (12)$$

If the medium above the reflector is homogeneous and the difference between the group and phase angles can be neglected, equation 12 provides an estimate of the offset $x_{\rm pr}$ of the polarity reversal:

$$\frac{x_{\rm pr}(\alpha)}{h} \;\approx\; 2\tan\theta_{\rm pr} \;=\; \frac{2}{\sqrt{-(1 \,+\, K^{(1)}\,\sin^2\alpha \,+\, K^{(2)}\,\cos^2\alpha)}}\,, \qquad (13)$$

where h is the depth of the reflector.

3.2.1 Model 1

The first test was performed for a boundary between orthorhombic (top) and isotropic (bottom) halfspaces (Figure 5). Both media have the same vertical velocities and densities as those in the VTI/isotropic model analyzed above (see Table 2 and Figures 2–4). Also, the anisotropy parameters in the symmetry plane $[x_1, x_3]$ of the orthorhombic medium are taken from the VTI model in Table 2. Although the medium above the reflector is azimuthally anisotropic, the offset of the polarity reversal is weakly dependent on azimuth (Figure 5).

The initial model for 3D analysis of the long-spread gather was obtained by first estimating the NMO ellipse on conventional-spread data and then processing long-offset data (for the maximum offset-to-depth ratio $x_{\rm max}/h = 2$) in narrow sectors centered at the vertical symmetry planes. The NMO ellipse reconstructed by the conventional semblance operator for offset-to-depth ratios limited by unity has the correct orientation but highly distorted semi-axes equal to 3.20 km/s and 3.44 km/s (the actual values are 2.66 km/s and 2.87 km/s); the semblance is only 0.45. Clearly, conventional pro-

Table 3. Parameters of a model that includes orthorhombic (top) and isotropic (bottom) media. The P-wave reflection from this interface has an azimuthally varying type 2 AVO response.

	Layer 1	Layer 2
Symmetry type	ORTH	ISO
Density (g/cm^3)	2.43	2.14
V_{P0} (km/s)	2.96	3.49
V_{S0} (km/s)	1.38	2.29
$\epsilon^{(1)}$	0.065	0
$\delta^{(1)}$	-0.029	0
$\gamma^{(1)}$	0.18	0
$\epsilon^{(2)}$	0.065	0
$\delta^{(2)}$	-0.096	0
$\gamma^{(2)}$	0.05	0
$\delta^{(3)}$	-0.08	0
$V_{\rm nmo}^{(1)}$	2.87	3.49
$V_{\rm nmo}^{(2)}$	2.66	3.49
$\eta^{(1)}$	0.10	0
$\eta^{(2)}$	0.20	0
$\eta^{(3)}$	0.10	0

cessing cannot be used for either stacking of the wide-azimuth data or inversion of NMO ellipses.

The final inversion results for two spreadlengths ($x_{\rm max}/h = 2$ and $x_{\rm max}/h = 3$) are displayed in Figure 6. Note that with both conventional and AK semblance, the parameters for the $[x_1, x_3]$ symmetry plane estimated from the 3D inversion almost coincide with those obtained for the VTI model in Figure 4. Because of the influence of the polarity reversal, conventional semblance produces highly distorted NMO velocities and η values for both spreadlengths and the full range of azimuths. For type 2 AVO with small values of $x_{\rm pr}$, muting out long offsets does not help the conventional algorithm to reconstruct the NMO ellipse. As was the case for the VTI model, AK semblance correctly compensates for the polarity reversal and gives accurate estimates of the azimuthally varying parameters $V_{\rm nmo}$ and η.

3.2.2 Model 2

For the second test we chose another type 2 AVO model, for which the offset $x_{\rm pr}$ of the polarity reversal is larger and varies more strongly with azimuth (Figure 7). The normalized offset $x_{\rm pr}/h$ changes from 0.65 in the $[x_1, x_3]$ symmetry plane ($\alpha = 0^\circ$) to 0.85 in the $[x_1, x_3]$-plane ($\alpha = 90^\circ$).

The NMO ellipse reconstructed by the conventional method for offsets limited by the reflector depth has the correct orientation and the semi-axes 2.43 km/s and 2.11 km/s (the actual values are 2.53 km/s and 2.16 km/s); the semblance is 0.6. The accuracy achieved by the conventional method is explained by the relatively large (for type 2 AVO) offsets $x_{\rm pr}(\alpha)$ of the polarity reversal and low reflection amplitudes for $x > x_{\rm pr}$.

Application of the AK algorithm, however, becomes necessary for long-offset data because conventional semblance yields highly erroneous η values (Figures 8b,d). As discussed above, we obtain the initial model for 3D analysis by first estimating the NMO ellipse on conventional-spread data with $K^{(1)} = K^{(2)} = K$ and then processing long-offset data near the vertical symmetry planes, which gives $K^{(1)} = -5.85$ and $K^{(2)} = -6.21$. The results of 3D nonhyperbolic AK semblance analysis for two long spreads are shown in Figure 8. Since the polarity reversal now occurs in the smaller-offset half of the spread, conventional semblance produces a significant error not only in η, but also in the NMO ellipse. The η values estimated by the conventional algorithm for $x_{\rm max}/h = 2$ even become negative for a wide range of azimuths (Figure 8b).

The AK semblance method, which properly accounts for the azimuthally dependent polarity reversal, gives far superior results. There is practically no error in the reconstruction of the NMO ellipse, while the mild distortion in η for $x_{\rm max}/h = 2$ is caused by the small bias in the nonhyperbolic moveout equation (Tsvankin, 2005) and insufficient spreadlength. Since the parameter η controls nonhyperbolic moveout, it is better constrained for larger spreadlengths. When the maximum offset-to-depth ratio is increased from two to three (Figure 8d), the errors in the function $\eta(\alpha)$ become almost negligible.

3.3 3D semblance for type 1 AVO

Compared to the type 2 AVO response analyzed above, type 1 AVO is typically characterized by a higher normal-incidence reflection coefficient, and the polarity reversal is observed at larger offsets (Figure 1). As long as the polarity reversal does not occur in the recorded offset range, the data can be processed by the conventional semblance algorithm. However, for long-spread reflections with offset-to-depth ratios reaching two, the offset $x_{\rm pr}$ may be close to middle of the spread. Anisotropy, in particular, tends to move the polarity reversal toward smaller offsets (Figure 1).

Figure 9 displays a P-wave reflection from an interface between orthorhombic and isotropic media (see Table 5). The event has a typical type 1 AVO response, with the polarity reversal recorded at offset-to-depth ratios of about 1.2. Although the conventional algorithm performs better than it did for type 2 AVO, the errors in both the NMO ellipse and parameter η are noticeable (Figure 10). A more accurate reconstruction of the NMO ellipse using conventional semblance can be achieved by reducing the maximum offset-to-depth ratio to $x_{\rm max}/h < 1.2$ (i.e., by truncating the spread before the polarity reversal). Despite the presence of

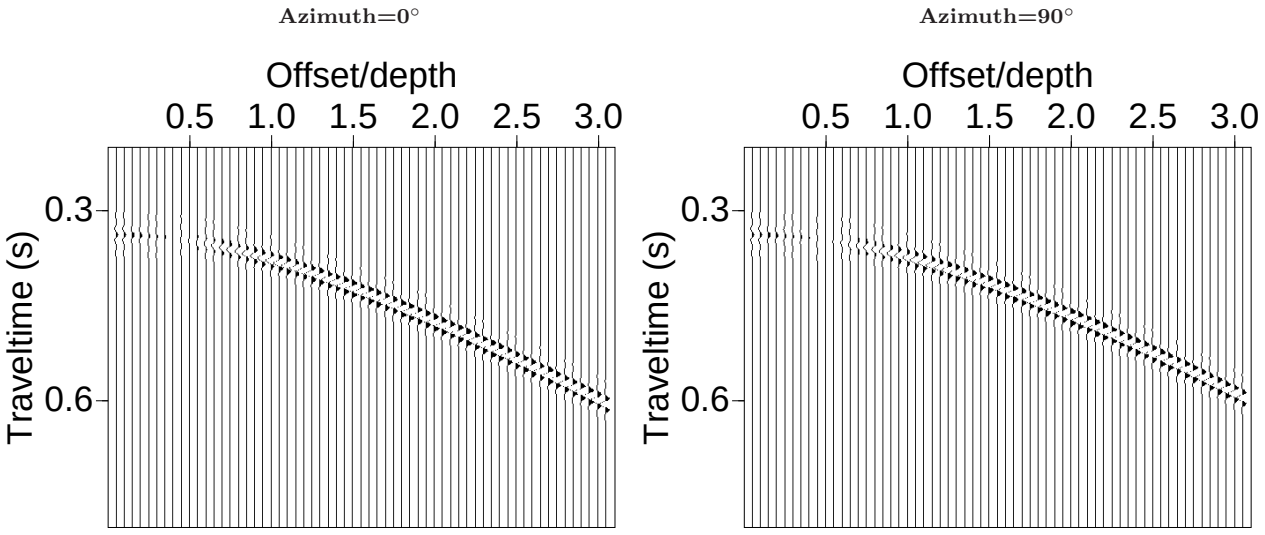

Figure 5. Shot records of a P-wave reflection from an orthorhombic/isotropic interface with a type 2 AVO response (Table 3). The seismograms are computed for the symmetry planes $[x_1, x_3]$ ($\alpha = 0°$) and $[x_2, x_3]$ ($\alpha = 90°$).

Table 4. Orthorhombic/orthorhombic model for which the P-wave reflection has an azimuthally varying type 2 AVO response. The two media have the same orientation of the vertical symmetry planes. Compared to the model from Table 3, the polarity reversal occurs at larger offsets.

	Layer 1	Layer 2
Symmetry type	ORTH	ORTH
Density (g/cm^3)	2.4	2.5
V_{P0} (km/s)	2.35	2.50
V_{S0} (km/s)	1.41	1.83
$\epsilon^{(1)}$	0.20	0.16
$\delta^{(1)}$	0.08	0.09
$\gamma^{(1)}$	0.18	0.05
$\epsilon^{(2)}$	0.13	0.09
$\delta^{(2)}$	-0.08	-0.07
$\gamma^{(2)}$	0.05	0.03
$\delta^{(3)}$	-0.08	-0.09
$V_{\rm nmo}^{(1)}$	2.53	2.72
$V_{\rm nmo}^{(2)}$	2.16	2.32
$\eta^{(1)}$	0.10	0.09
$\eta^{(2)}$	0.25	0.19
$\eta^{(3)}$	0.07	0.14

Table 5. Orthorhombic/isotropic model for which the P-wave reflection has an azimuthally varying type 1 AVO response.

	Layer 1	Layer 2
Symmetry type	ORTH	ISO
Density (g/cm^3)	2.4	2.6
V_{P0} (km/s)	3.30	3.84
V_{S0} (km/s)	1.45	2.46
$\epsilon^{(1)}$	0.20	0
$\delta^{(1)}$	0.10	0
$\gamma^{(1)}$	0.20	0
$\epsilon^{(2)}$	0.13	0
$\delta^{(2)}$	-0.10	0
$\gamma^{(2)}$	0.05	0
$\delta^{(3)}$	0.02	0
$V_{\rm nmo}^{(1)}$	3.61	3.84
$V_{\rm nmo}^{(2)}$	2.95	3.84
$\eta^{(1)}$	0.08	0
$\eta^{(2)}$	0.29	0
$\eta^{(3)}$	0.07	0

the polarity reversal, the error in the NMO ellipse obtained by the AK semblance is almost negligible for both spreadlengths (Figures 10a,c).

As was the case for type 2 AVO (see Figure 8), the AK semblance operator gives a higher accuracy in η for the longer spread ($x_{\rm max}/h = 3$), especially in the $[x_1, x_3]$-plane where $\eta(\alpha)$ reaches its maximum (Figures 10b,d). Somewhat suprisingly, the η estimate produced by the conventional semblance deteriorates with increasing spreadlength. This reduction in accuracy is most likely explained by the increased distortion caused by the polarity reversal on longer spreads, as the semblance becomes more influenced by traces at large (post-reversal) offsets $x > x_{\rm pr}$.

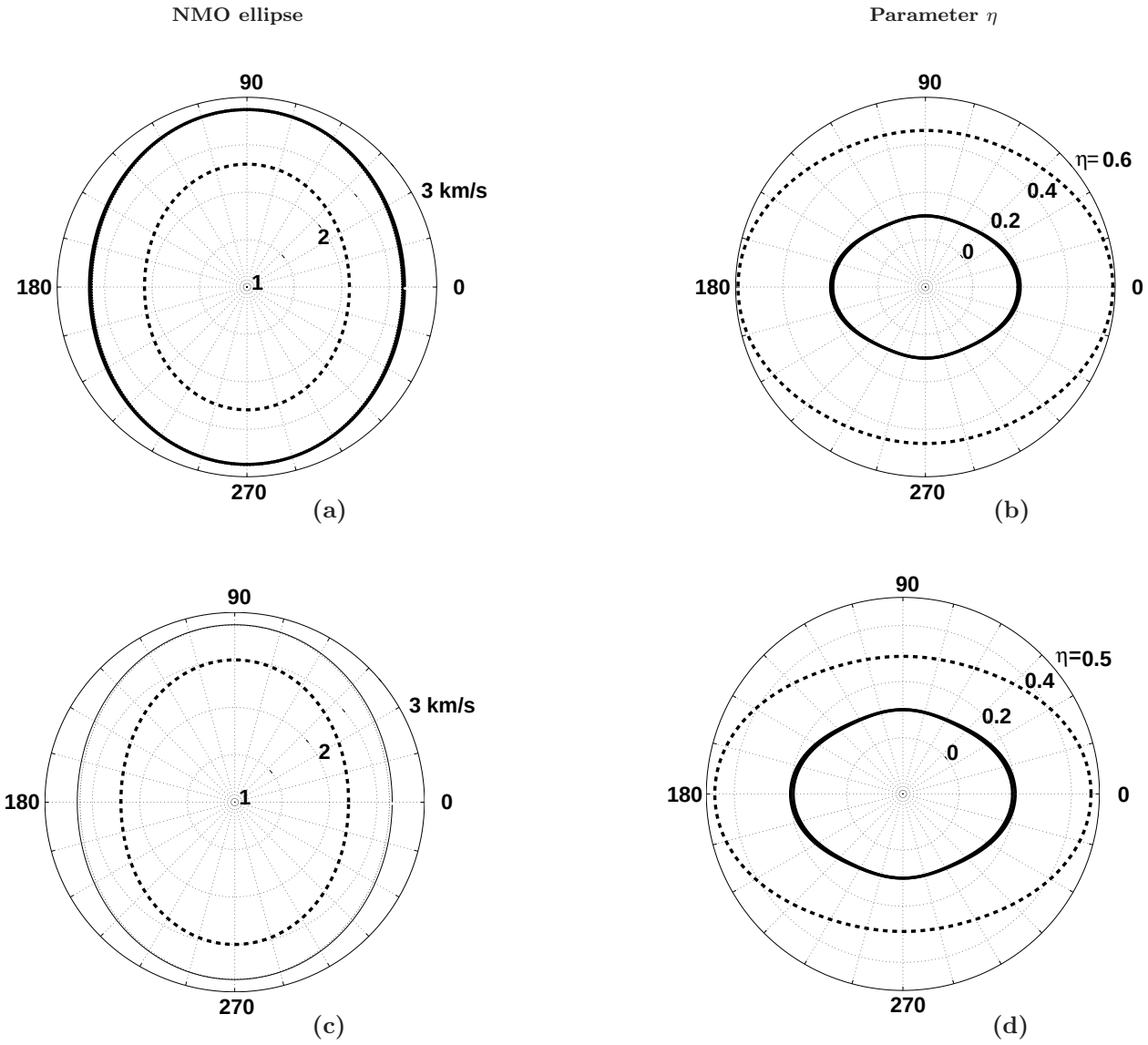

Figure 6. Moveout-inversion results for a wide-azimuth, long-offset P-wave reflection from an orthorhombic/isotropic interface (Table 3). The event has a type 2 AVO response with the polarity reversal at offset-to-depth ratios close to 0.5. (a) and (c) are the NMO ellipses; (b) and (d) are the azimuthally-dependent η values. The maximum offset-to-depth ratio is two for the top row, and three for the bottom row. The solid lines are the actual NMO ellipses and η-curves, the dashed lines are estimated by the conventional semblance algorithm, and the dotted lines by AK semblance. Since the AK semblance algorithm reconstructs the moveout parameters with high accuracy, the dotted lines are almost invisible. The azimuth with respect to the symmetry plane $[x_1, x_3]$ is shown on the perimeter.

4 DISCUSSION

Our results demonstrate that a smooth amplitude function based on Shuey's equation for the AVO gradient is sufficient for removing the influence of polarity reversals on semblance analysis. Still, it should be emphasized that AK semblance should not be regarded as a substitute for 2D or 3D (azimuthal) AVO analysis. Whereas the small-offset AVO equation used in our algorithm is sufficient to correct for the phase change of the wavelet in the presence of polarity reversals, it gives a rather crude approximation for reflection amplitudes on long spreads. Also, it does not properly account for propagation phenomena, such as geometrical spreading and transmission coefficients along the raypath. Therefore, the role of the AK semblance method

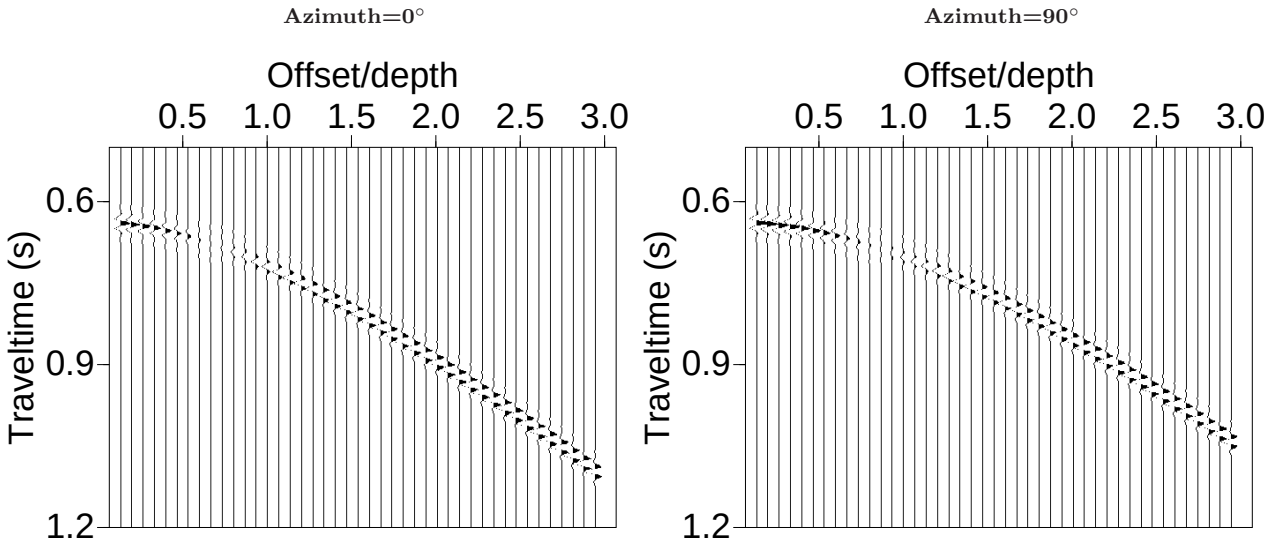

Figure 7. Shot records of a P-wave reflection from an orthorhombic/orthorhombic interface with a type 2 AVO response (Table 4). The seismograms are computed for the symmetry planes $[x_1, x_3]$ ($\alpha = 0°$) and $[x_2, x_3]$ ($\alpha = 90°$). The offset of the polarity reversal for this model noticeably varies with azimuth.

is limited to estimating an accurate set of parameters that control the nonhyperbolic moveout equation. The robust moveout inversion ensures the flatness of multi-azimuth, long-spread events prior to stacking and amplitude picking. The moveout parameters also serve as the input to the anisotropic geometrical-spreading correction (Xu and Tsvankin, 2006a, 2006b) that should be applied prior to AVO analysis.

Far-offset amplitudes needed in our algorithm often are too low to make a meaningful contribution to the semblance operator. Therefore, it may be necessary to gain the whole data set as a prerequisite to stable AK semblance computation. This preprocessing step can be accomplished with any empirical gain function. As mentioned above, a more accurate geometrical-spreading correction can be implemented after the moveout inversion.

In some of our tests for models with large velocity contrasts and type 1 AVO response, the critical angle was small enough for long-spread gathers to include post-critical offsets. As discussed in detail by Landrø and Tsvankin (2007), the critical angle for orthorhombic media varies with azimuth and can be used in anisotropic parameter estimation. According to Sarkar et al. (2002), the phase change with offset at the critical angle does not lead to significant errors in stacking velocity when the hyperbolic moveout equation is used in the semblance computation. However, our numerical tests show that the influence of the critical angle causes severe distortions in the η values estimated by the 3D AK semblance operator. Therefore, it is essential to mute out post-critical offsets in AK nonhyperbolic semblance analysis.

Although the numerical examples here were generated for two-layer models, the AK semblance algorithm can be applied in the same way to multilayered VTI and orthorhombic media. In the presence of vertical heterogeneity, the estimated moveout parameters represent effective quantities for the medium above the reflector (Vasconcelos and Tsvankin, 2006). Also, it should be mentioned that AK semblance cannot help to resolve the tradeoffs between NMO velocities and η parameters discussed in detail by Tsvankin (2005) and Vasconcelos and Tsvankin (2006).

5 CONCLUSIONS

Polarity reversals, which may be quite common for long-spread gathers of reflection events, can produce significant distortions in velocity estimation using conventional semblance analysis. Here, we presented an efficient AVO-sensitive methodology designed to account for the influence of polarity reversals on moveout inversion for long-offset 2D and 3D (wide-azimuth) P-wave reflection data. The 2D algorithm is based on the Alkhalifah-Tsvankin nonhyperbolic moveout equation that accurately describes P-wave traveltimes in vertical symmetry planes of layered anisotropic media. Following the so-called "AK semblance" method of Sarkar et al., the amplitude variation with offset is approximated by a two-parameter function that reduces to Shuey's AVO equation when the overburden is isotropic and homogeneous. To minimize the tradeoffs between the

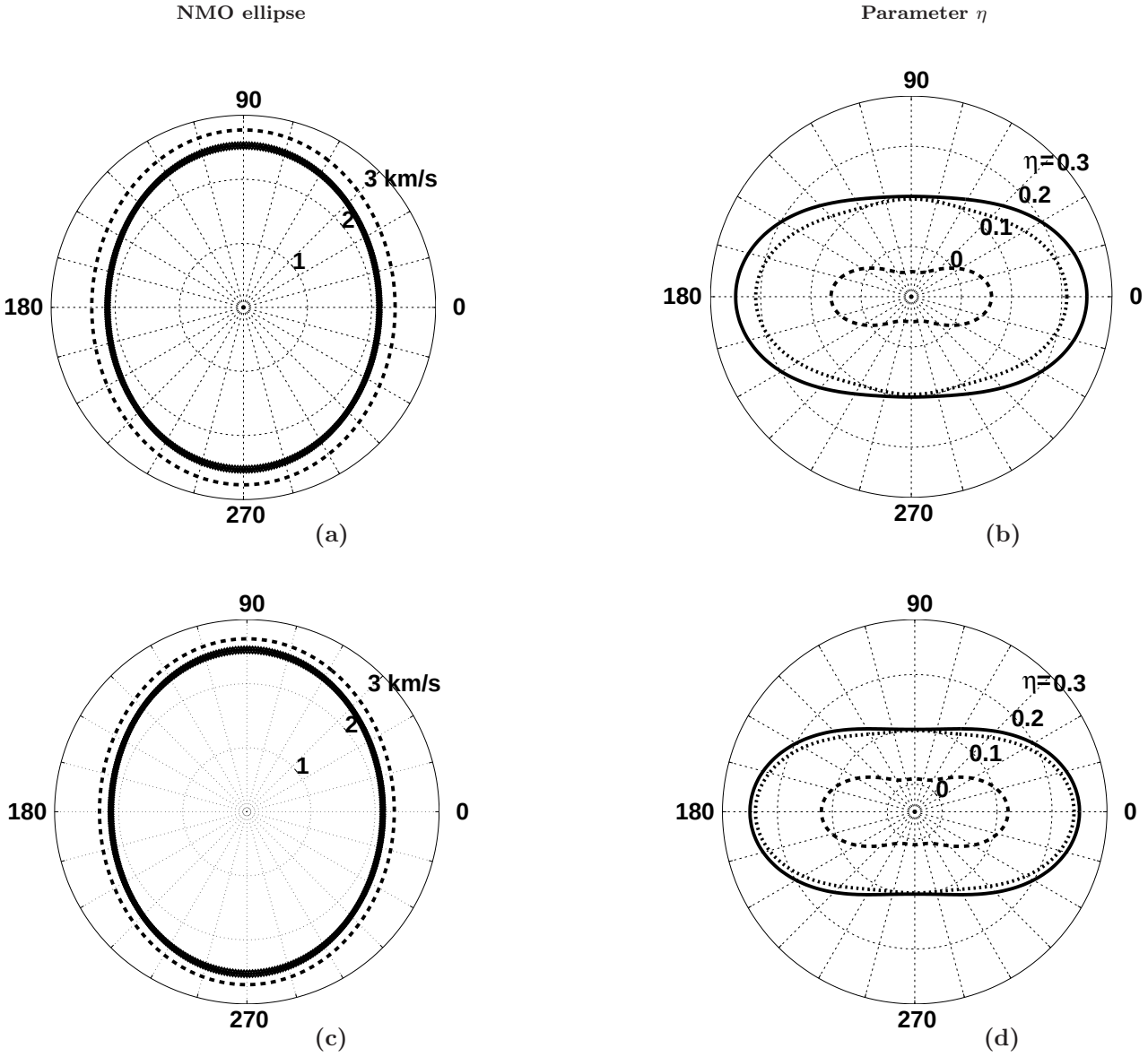

Figure 8. Moveout-inversion results for a wide-azimuth, long-offset P-wave reflection from an orthorhombic/orthorhombic interface (Table 4). The event has a type 2 AVO response with the polarity reversal at offsets between $x/h = 0.65$ and $x/h = 0.85$. The maximum offset-to-depth ratio is two for the top row, and three for the bottom row. The solid lines are the actual NMO ellipses and η-curves, the dashed lines are estimated by the conventional semblance algorithm, and the dotted lines by AK semblance [the dotted and solid curves in plots (a) and (c) almost coincide].

model parameters, the ratio of the AVO gradient and intercept ($K = A/B$) for each reflection event is kept constant.

Although the employed amplitude dependence does not include geometrical spreading and higher-order AVO terms, it proved sufficiently accurate for purposes of moveout inversion. Synthetic tests on long-offset P-wave data from VTI media show that conventional semblance breaks down for type 2 AVO responses with the polarity reversal at relatively small offsets-to-depth ratios (less than unity). Even when combined with the Alkhalifah-Tsvankin equation, the conventional semblance operator produces errors in the NMO velocity and completely distorts the key time-processing parameter η. These errors are practically eliminated by the AK semblance operator, which achieves the same high accuracy in the estimates of $V_{\rm nmo}$ and η as that for AVO-free events.

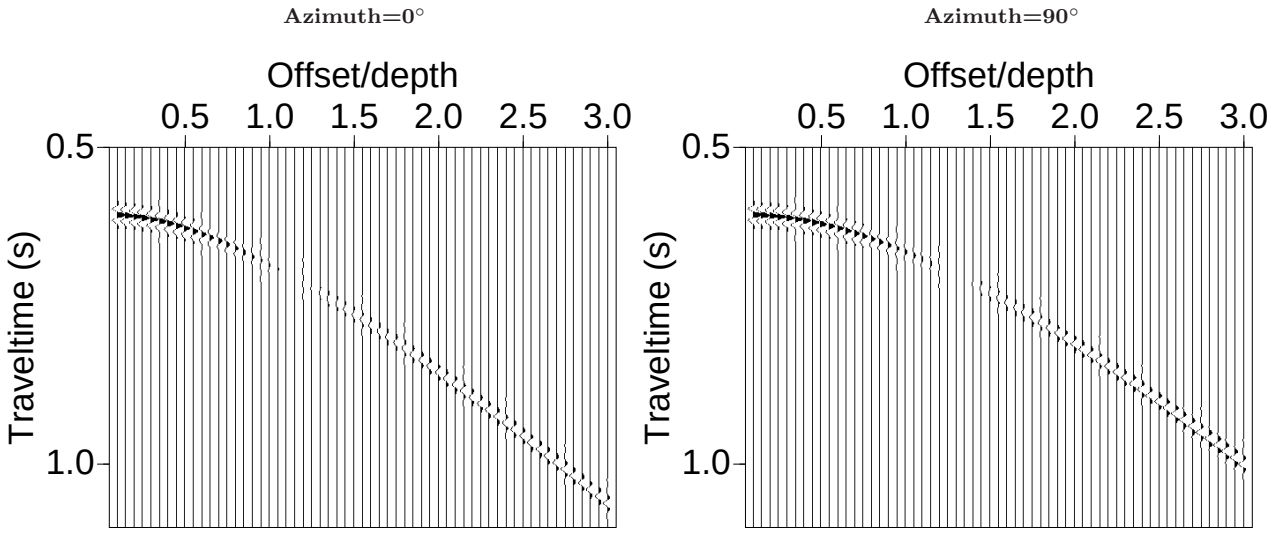

Figure 9. Shot records of a P-wave reflection from an orthorhombic/isotropic interface with a type 1 AVO response (Table 5). The seismograms are computed for the symmetry planes $[x_1, x_3]$ ($\alpha = 0°$) and $[x_2, x_3]$ ($\alpha = 90°$).

Despite the addition of the amplitude parameters (A, which is defined at each time sample, and K), the 2D AK semblance algorithm is computationally efficient because the best-fit values of A and K are obtained analytically by differentiating the semblance function. As a result, the scanning is carried out only over the same two moveout parameters ($V_{\rm nmo}$ and η) as in the conventional method. The only difference between the AK and conventional algorithms in terms of computational cost is in the more complicated form of the AVO-sensitive semblance operator.

For 3D wide-azimuth data, AK semblance needs to handle azimuthally dependent amplitudes, which are largely governed by the AVO gradient. The amplitude function in our 3D AK semblance operator is based on the azimuthal variation of the AVO gradient for orthorhombic media. This amplitude dependence, which is controlled by the symmetry-plane values of K ($K^{(1)}$ and $K^{(2)}$), was incorporated into a nonhyperbolic moveout inversion algorithm for wide-azimuth data that operates with a generalized form of the Alkhalifah-Tsvankin equation. The 3D AK semblance is designed to invert for $K^{(1)}$ and $K^{(2)}$ along with the moveout parameters of orthorhombic media, which include the azimuth of one of the symmetry planes, two symmetry-plane NMO velocities and three η coefficients ($\eta^{(1,2,3)}$). To start the semblance search with an accurate initial model, the multidimensional scan on the full 3D gather is preceded by estimation of the NMO ellipse and by 2D inversion of long-offset data near the symmetry-plane directions.

The improvement achieved by the 3D AK semblance is especially significant for orthorhombic models with type 2 AVO response. The conventional method completely breaks down on long spreads and even produces η values that have the wrong sign. Despite the approximate nature of its amplitude function, the AK semblance algorithm properly accounts for the azimuthally varying polarity reversal in the estimation of both the NMO ellipse and the η-curve. For type 1 AVO, the polarity reversal occurs at larger offsets (typically, at offset-to-depth ratios larger than unity), which makes the conventional method more accurate. Still, since inversion for η requires offsets reaching at least two reflector depths, the polarity reversal distorts the output of the conventional semblance operator. As is the case for AVO-free data, the accuracy of the η parameters computed by the AK semblance algorithm increases for larger spreadlengths. In contrast, conventional semblance for type 1 AVO gives more distorted η estimates with increasing spreadlength, as the influence of the polarity reversal becomes more substantial.

On the whole, nonhyperbolic moveout inversion for both type 1 and type 2 AVO response should be performed with the AVO-sensitive semblance operator. While it may be possible to reconstruct the NMO ellipse by applying conventional semblance to a truncated gather (mostly for type 1 AVO), accurate estimation of the η-parameters requires application of AK semblance. Note that in combination with the symmetry-plane NMO velocities, the parameters $\eta^{(1,2,3)}$ control time processing and geometrical spreading of P-wave data in orthorhombic media.

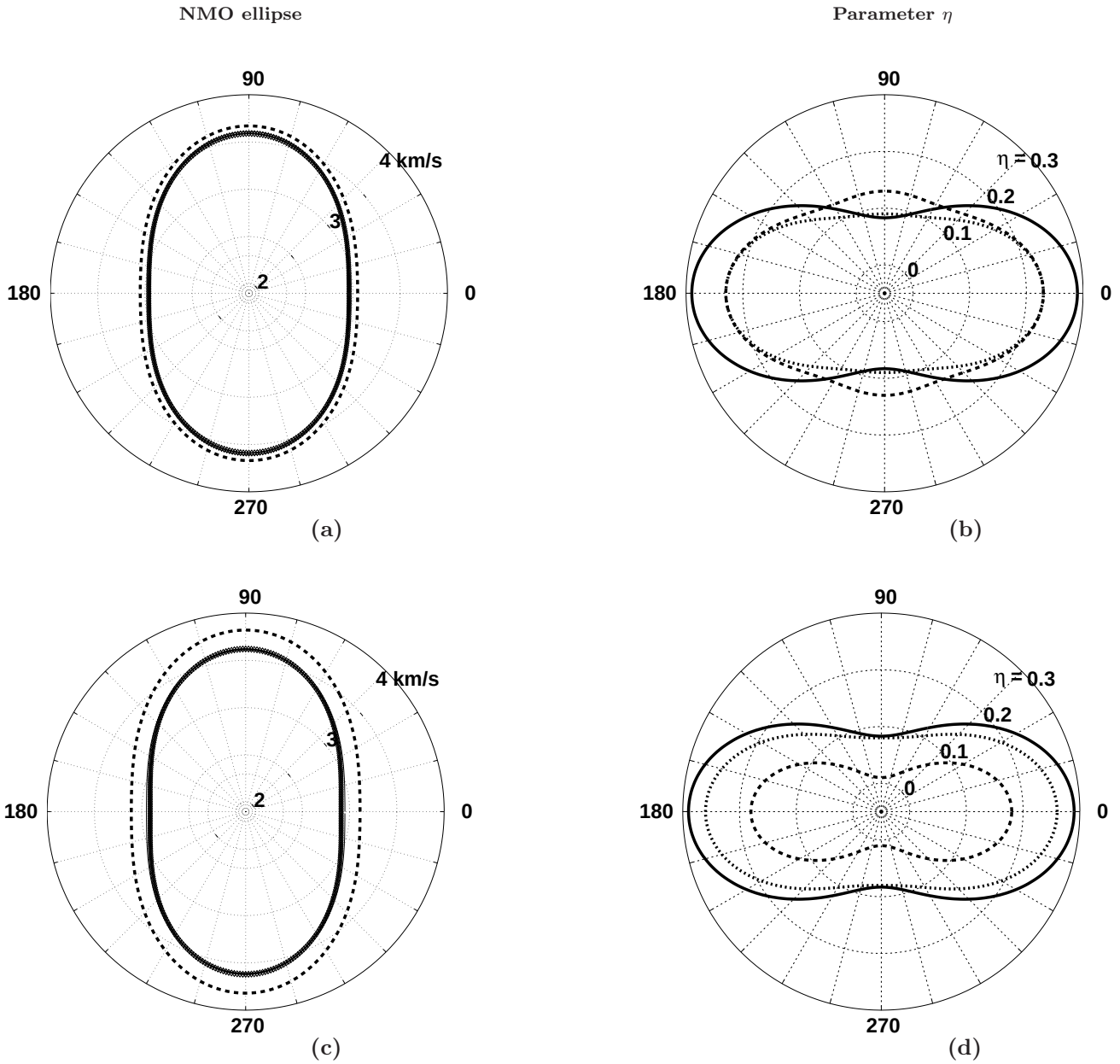

Figure 10. Moveout-inversion results for a wide-azimuth, long-offset P-wave reflection from an orthorhombic/isotropic interface (Table 5). The event has a type 1 AVO response with the polarity reversal at offsets between $x/h = 1$ and $x/h = 1.5$. (a) and (c) are the NMO ellipses; (b) and (d) are the azimuthally-dependent η values. The maximum offset-to-depth ratio is two for the top row, and three for the bottom row. The solid lines are the actual NMO ellipses and η-curves, the dashed lines are estimated by the conventional semblance algorithm, and the dotted lines by AK semblance. As in Figure 6, the dotted lines in plots (a,c) are almost invisible.

6 ACKNOWLEDGMENTS

We are grateful to the A(nisotropy)-Team of the Center for Wave Phenomena (CWP), Colorado School of Mines (CSM), for helpful discussions. We would like to thank Debashish Sarkar (GX Technology) and Ivan Vasconcelos (CSM) for providing their codes, which were critically important for the success of this study. This work was supported by the Consortium Project on Seismic Inverse Methods for Complex Structures at CWP and by the Chemical Sciences, Geosciences and Biosciences Division, Office of Basic Energy Sciences, Office of Science, U.S. Department of Energy.

REFERENCES

Alkalifah, T., and I. Tsvankin, 1995, Velocity analysis for transversely isotropic media: Geophysics, **60**, 1550–1566.

Bakulin, A., V. Grechka, and I. Tsvankin, 2000, Estimation of fracture parameters from reflection seismic data – Part II: Fractured models with orthorhombic symmetry: Geophysics, **65**, 1803–1817.

Gajewski, D., and I. Pšenčík, 1987, Computation of high frequency seismic wavefields in 3-D laterally inhomogeneous anisotropic media: Geophysical Journal of the Royal Astronomical Society, **91**, 383–412.

Grechka, V., and M. Kachanov, 2006, Seismic characterization of multiple fracture sets: Does orthotropy suffice? Geophysics, **71**, D93–D105.

Kim, K. Y., K. H. Wrolstad, and F. Aminzadeh, 1993, Effects of transverse isotropy on P-wave AVO for gas sands: Geophysics, **58**, 883–888.

Landrø, M., and I. Tsvankin, 2007, Seismic critical-angle reflectometry: A method to characterize azimuthal anisotropy?: Geophysics, in print.

Pech, A., and I. Tsvankin, 2004, Quartic moveout coefficient for a dipping azimuthally anisotropic layer: Geophysics, **69**, 699–707.

Press, W. H., S. A. Teukolsky, W. T. Vetterling, and B. P. Flannery, 1992, Numerical Recipes in C: The art of scientific computing: Cambridge University Press.

Rüger, A., 2001, Reflection coefficients and azimuthal AVO analysis in anisotropic media: Society of Exploration Geophysicists.

Rutherford, S., and R. Williams, 1989, Amplitude-versus-offset variations in gas sands: Geophysics, **54**, 680–688.

Sarkar, D., R. T. Baumel, and K. Larner, 2002, Velocity analysis in the presence of amplitude variation: Geophysics, **67**, 1664–1672.

Sarkar, D., J. P. Castagna, and W. Lamb, 2001, AVO and velocity analysis: Geophysics, **66**, 1284–1293.

Schoenberg M. and K. Helbig, 1997, Orthorhombic media: Modeling elastic wave behavior in a vertically fractured earth: Geophysics, **62**, 1954–1974.

Shuey, R. T, 1985, A simplification of the Zoeppritz equations: Geophysics, **50**, 609–614.

Taner, M. T., and F. Koehler, 1969, Velocity spectra – digital computer derivation and applications of velocity functions: Geophysics, **34**, 859–881.

Thomsen, L., 1986, Weak elastic anisotropy: Geophysics, **51**, 1954–1966.

Tsvankin, I., 1997, Anisotropic parameters and P-wave velocity for orthorhombic media: Geophysics, **62**, 1292–1309.

Tsvankin, I., 2005, Seismic signatures and analysis of reflection data in anisotropic media, 2nd edition: Elsevier Science Publ. Co., Inc.

Tsvankin, I., and L. Thomsen, 1994, Nonhyperbolic reflection moveout in anisotropic media: Geophysics, **59**, 1290–1304.

Vasconcelos, I., and I. Tsvankin, 2006, Non-hyperbolic moveout inversion of wide-azimuth P-wave data for orthorhombic media: Geophysical Prospecting, **54**, 535–552.

Xu, X., and I. Tsvankin, 2006a, Anisotropic geometrical-spreading correction for wide-azimuth P-wave reflections: Geophysics, **71**, D161–D170.

Xu, X., and I. Tsvankin, 2006b, Azimuthal AVO analysis with anisotropic spreading correction: A synthetic study: The Leading Edge, **24**, 1336–1342.

Zhu, Y., and I. Tsvankin, 2006, Plane-wave propagation in attenuative transversely isotropic media: Geophysics, **71**, T17–T30.

APPENDIX A: THE 2D AND 3D AK SEMBLANCE OPERATORS

A1 AK semblance in 2D

Conventional semblance operators are based on summation of trace amplitudes along moveout curves (which usually are hyperbolic) within a certain time window. The idea of amplitude-sensitive semblance is to replace this summation with data *modeling* using a moveout equation in combination with an amplitude function $M(t_1, x)$, where t_1 is the zero-offset time and x is the source-receiver offset. The amplitude function for AK semblance is specified as (Sarkar et al., 2002)

$$M_x(t_1) = A(t_1)\left(1 + K\sin^2\theta_x\right), \tag{A1}$$

where $A(t_1)$ is the AVO intercept, K is the ratio of AVO gradient and intercept (K is kept constant inside the semblance window), and θ_x is the incidence angle at offset x approximately given by

$$\sin^2\theta_x = \frac{x^2}{x^2 + V_{\rm nmo}^2 t_0^2}. \tag{A2}$$

Here, $V_{\rm nmo}$ is the NMO velocity and t_0 is the zero-offset time at the center of the semblance window.

Following Sarkar et al. (2002), we define the 2D AK semblance operator as

$$S_G(t_0) = 1 - \frac{\sum_{t_1}\sum_{x}\left[A(t_1)\left(1 + K\sin^2\theta_x\right) - D_V(t_1, x)\right]^2}{\sum_{t_1}\sum_{x} D_V^2(t_1, x)}, \tag{A3}$$

where $D_V = D_V(t_1, x)$ is the moveout-corrected data at the zero-offset time t_1; the summation is carried out over all offsets x and all time samples within the semblance window centered at t_0. The subscript "V" denotes the trial NMO velocity $V_{\rm nmo}$ used by Sarkar et al. (2002) to perform the conventional hyperbolic moveout correction. In our algorithm, the data are modeled using a nonhyperbolic moveout equation parameterized by $V_{\rm nmo}$ and the anellipticity coefficient η (see the main text).

The value of the AVO intercept that corresponds to the maximum of the generalized semblance function can

be found by setting to zero the derivative of equation A3 with respect to $A(t_1)$:

$$A(t_1) = \frac{\sum_x \left[D_V(t_1,x)\ \left(1 + K\sin^2\theta_x\right)\right]}{\sum_x \left(1 + K\sin^2\theta_x\right)^2}\,. \tag{A4}$$

Substituting $A(t_1)$ from equation A4 into equation A3 yields

$$S_G(t_0) = \frac{\sum_{t_1}\left[\sum_x D_V(t_1,x)\ \left(1 + K\sin^2\theta_x\right)\right]^2}{\sum_x (1 + K\sin^2\theta_x)^2 \sum_{t_1}\sum_x D_V^2(t_1,x)}\,. \tag{A5}$$

Similarly, next we differentiate S_G (equation A5) with respect to K and set the derivative to zero:

$$\alpha K^2 - \beta K + \gamma = 0\,, \tag{A6}$$

where

$$\begin{aligned}\alpha &= \sum_x \sin^2\theta_x \sum_{t_1}\left(\sum_x D_V(t_1,x)\ \sin^2\theta_x\right)^2 \\ &- \sum_x \sin^2\theta_x \\ &\times \sum_{t_1}\left[\sum_x D_V(t_1,x)\sum_x \left(D_V(t_1,x)\ \sin^2\theta_x\right)\right],\end{aligned} \tag{A7}$$

$$\begin{aligned}\beta &= \sum_x \sin^2\theta_x \sum_{t_1}\left(\sum_x D_V(t_1,x)\right)^2 \\ &- N\sum_{t_1}\left(\sum_x D_V(t_1,x)\ \sin^2\theta_x\right)^2,\end{aligned} \tag{A8}$$

$$\begin{aligned}\gamma &= N\sum_{t_1}\left[\sum_x D_V(t_1,x)\sum_x \left(D_V(t_1,x)\ \sin^2\theta_x\right)\right] \\ &- \sum_x \sin^2\theta_x \sum_{t_1}\left(\sum_x D_V(t_1,x)\right)^2.\end{aligned} \tag{A9}$$

The solution of the quadratic equation A6 that always maximizes the semblance for both positive and negative values of α is (Sarkar et al., 2002)

$$K = \frac{\beta - \sqrt{\beta^2 - 4\alpha\gamma}}{2\alpha}\,. \tag{A10}$$

Substituting K from equation A10 into equation A5, we obtain the 2D generalized semblance operator that depends only on the parameters of the moveout function.

A2 AK semblance in 3D

Here, the AK semblance operator is extended to long-offset 3D data collected into common-midpoint (CMP) gathers with a wide range of source-receiver azimuths. The 3D AK semblance is computed from equation A3 where the summation is performed not only over all offsets, but also over all azimuths α. Setting the derivative of $S_G(t_0)$ with respect to A_1 to zero, we obtain the generalized 3D semblance in a form similar to equation A5:

$$\begin{aligned}&S_G(t_0) \\ &= \frac{\sum_{t_1}\left[\sum_x\sum_\alpha D_V(t_1,x,\alpha)\ \left(1 + K(\alpha)\sin^2\theta_x\right)\right]^2}{\sum_x\sum_\alpha (1 + K(\alpha)\sin^2\theta_x)^2 \sum_{t_1}\sum_x\sum_\alpha D_V^2(t_1,x,\alpha)}\,.\end{aligned} \tag{A11}$$

The incidence angle θ_x is expressed through offset using equation A2. As discussed in the main text, the function $K(\alpha)$ is based on the azimuthal dependence of the AVO gradient in orthorhombic media:

$$K(\alpha) = K^{(2)}\cos^2\alpha + K^{(1)}\sin^2\alpha\,, \tag{A12}$$

where the azimuth α is defined with respect to the $[x_1, x_3]$ symmetry plane.

Since in the 3D case it is difficult to obtain the best-fit values of $K^{(1)}$ and $K^{(2)}$ analytically, they are estimated from the semblance scan using equation A11. For orthorhombic media, we employ a nonhyperbolic moveout equation parameterized by the azimuth of the $[x_1, x_3]$ symmetry plane, the NMO velocities $V_{\rm nmo}^{(1)}$ and $V_{\rm nmo}^{(2)}$, and the anellipticity coefficients $\eta^{(1)}$, $\eta^{(2)}$, and $\eta^{(3)}$. Therefore, semblance scanning is performed over a total of eight independent parameters. The semblance algorithm, which is based on the 3D nonhyperbolic moveout inversion technique of Vasconcelos and Tsvankin (2006), is described in more detail in the main text.